Composite Control Law for Nonlinear Systems with Mismatched Disturbances for a Ball-Ramp Dual-Clutch Transmission

Dong-Hyun Kim and Seibum B. Choi, *Member, IEEE,*

***Abstract*—The dual-clutch transmission (DCT) was developed to increase the transmission efficiency and the shift performance. However, in a DCT, due to uncertainty related to the actuator, the tie-up phenomenon can arise, in which two clutches engage together or the clutch torque control performance deteriorates. Especially, the actuator uncertainty increased when using a special mechanism to increase controllability and efficiency. Among them, the ball-ramp DCT (BR-DCT), which uses a self-energizing mechanism, can reduce the consumption of actuator energy while also reducing the tie-up effect. However, the nonlinearity of the actuator must be considered, such as friction between parts and change in friction coefficient. Among the methods by which this type of uncertainty is estimated, the nonlinear disturbance observer is most effective when used to estimate the unmodeled nonlinearity of an actuator and time-varying uncertainty. In order to execute disturbance rejection control to improve the performance of the shift controller using the estimated uncertainty, it is necessary to configure disturbance compensation input. However, because the BR-DCT powertrain includes mismatched disturbances and nonlinearity of the actuator, it is difficult to apply the existing methods on the composite control law to shift controller. Therefore, in this study, we propose a composite control law to guarantee integrated stability in nonlinear systems such as a BR-DCT powertrain. The proposed method was verified through a powertrain test bench equipped with a BR-DCT. Finally, the proposed composite control law was able to converge both the tracking error and the disturbance estimation error.**

***Index Terms*—Dual-clutch transmission, DCT, Shift Control, Disturbance Observer based Control, Composite Control Law, Nonlinear Disturbance Observer, Ball-ramp Mechanism**

I. Introduction

Many types of intelligent mobility systems have recently been spotlighted, but automobiles are still important. An automobile as an intelligent transportation means can be used as an autonomous driving system or an autonomous transportation system. In particular, in transportation systems that repeat similar routes, self-driving trucks are expected to achieve significant improvements in operational efficiency and cost. These autonomous transportation systems are used in many transportation industries, and it is expected that autonomous vehicles will account for a large proportion of all transportation vehicles in the future. Currently, vehicles in the autonomous transportation system are classified into internal combustion engine (ICE) vehicles, hybrid electric vehicles (HEV) and electric vehicles (EV) according to the type of power source. The EVs have low carbon emissions and good efficiency from energy source to wheels, but are very heavy due to high-capacity batteries, and well-to-wheel efficiency is not significantly improved compared to conventional ICEs. In addition, it is very expensive to manufacture the motor and battery, which are driving systems. HEV and ICE have larger carbon emissions than EVs, but their well-to-wheel efficiency is superior to or similar to that of EVs. In particular, HEV and ICE are driving systems with the lowest entry barrier at the present time, which is the initial stage of the autonomous transportation system, because the manufacturing unit cost is low due to mass production. Therefore, many autonomous transportation systems currently under development are based on ICE or HEV [1]–[3]. If the powertrain efficiency of these autonomous transport vehicles can be increased, the competitiveness of autonomous transport vehicles to be developed in the future can be further strengthened. Therefore, this paper deals with research on improving the efficiency of transmission applied to transportation systems.

The powertrain is a key element of a vehicle and directly affects the performance and efficiency. Among powertrain components, the transmission is a component that affects the energy efficiency and performance as much as the power source. In addition, performance and efficiency vary depending on the type of transmission. Early transmission studies began with the manual transmission (MT). A MT transmits power from the power source using a clutch, offering high transfer efficiency [4]. However, manipulation by the driver is required for shifting, and the acceleration performance can deteriorate due to the occurrence of a torque interruption, in which the drive torque falls to zero when the driver shifts [5]. The automated manual transmission (AMT) was studied to increase the convenience when the driver operates the vehicle. The AMT was able to increase the convenience by automating the operation of the clutch and the gear selector with an actuator [6]. However, torque interruption still occurred. In addition, given that an AMT uses a clutch similarly to a MT, the friction coefficient of the clutch changes according to the speed, torque, and temperature of the clutch. However, it is difficult to mount a sensor to measure the clutch torque due to cost and durability issues. As a result, the shift control performance when attempting to synchronize the speed of the power source and clutch deteriorated. That is, the shift speed

Seibum B. Choi is Professor at the School of Mechanical, Department of Mechanical Engineering, at the Korea Advanced Institute of Science and Technology (KAIST), 291 Daehak-ro, Yuseong-gu, Daejeon 305-338, Republic of Korea (e-mail: sbchoi@kaist.ac.kr).

Dong-Hyun Kim is Senior Research Engineer in R&D Division, Hyundai Motor Company, 150 HyundaiYeonguso-ro, Namyang-eup, Hwaseong-si, Gyeonggi-do, 18280, Republic of Korea (e-mail: kkddh@hyundai.com).

was slow or the shift shock felt by the driver increased.

The automatic transmission (AT) was developed to compensate for these shortcomings of the AMT. The AT improved the torque interruption issue by using a clutch-to-clutch (C2C) shift that crosses a clutch or brake connected to each gear [7]. In addition, in order to prevent the shift performance from deteriorating due to a change in the clutch friction coefficient, the AT uses a torque converter that transmits power through the viscosity of the fluid. The torque converter offers a comparative reduction in the shift shock due to the damping effect of fluid viscosity. In addition, an amplification effect occurred in that the power source rotates more rapidly than the transmission shaft at low speeds, allowing the launch performance to be improved. However, the overall fuel efficiency of the vehicle decreased somewhat due to the low transmission efficiency of the torque converter, and the shift time increased because the lock-up clutch had to be engaged after shifting [8], [9].

Recently, the dual-clutch transmission (DCT) has been actively studied to compensate for the shortcomings of the AT [10]–[15]. Because the DCT is equivalent to combining two AMTs, it is composed of a clutch connected to the odd gears and a clutch connected to the even gears [16]. Like the AT, C2C shifting is possible, meaning that the torque interruption issue could be eliminated. In addition, the fuel efficiency was improved given the use of a clutch with higher transmission efficiency than in the torque converter, and the shifting time was reduced because a lock-up clutch is not used. However, C2C shifting of a DCT can result in a tie-up condition in which the two clutches engage simultaneously [10]. When a tie-up occurs, a large amount of torque is applied to the shaft connected to each clutch, during which the shaft may be damaged. Nevertheless, precise shift control is difficult due to the change in the friction coefficient because the clutch torque remains difficult to measure. In particular, some DCT uses an actuator with a special mechanism to increase both the controllability and efficiency [11], [13], [14], [17]. This implies that if the lever ratio of the actuator is changed or an actuator model including a diaphragm spring is used, nonlinearity arises [17], [18]. In addition, if a self-energizing mechanism is used to reduce the actuator energy consumption or the tie-up effect, such as in a ball-ramp DCT (BR-DCT), nonlinearity arises in the actuator model [13], [14]. In such a case, the nonlinearity and uncertainty of the actuator should be considered along with the change in the friction coefficient.

To address these shortcomings, studies estimating the uncertainty of DCT have been conducted. First, a method of assuming uncertainty as a constant and updating at every shift by means of adaptation was proposed [19]. This method is suitable for estimating the change in the friction coefficient that occurs when the temperature of the clutch increases due to frequent shifting or due to the constant uncertainty of the actuator. However, in this case, it becomes difficult to estimate the rapid change in the friction coefficient according to the slip speed or torque of the clutch or the non-constant uncertainty of the actuator, and the modeling accuracy is reduced because the actuator is assumed to be a linear system. Second, a number of methods that estimate the change in the friction coefficient based on the observer have been proposed [20], [21]. These methods are suitable for estimating rapidly changing uncertainty levels. Additionally, in some studies, it was possible to estimate effectively the non-constant uncertainty of an actuator using a nonlinear actuator model, assuming that the uncertainty varied over time [22]. As such, various methods by which to estimate the uncertainty have been studied to improve the shifting performance of a DCT. Among them, studies using disturbance observers have shown the best performance when there is nonlinearity of the actuator or when uncertainties are non-constant. Therefore, in this study, an uncertainty estimation method using a disturbance observer is used.

In order to compensate for and remove the estimated uncertainty in the shift controller, it is necessary to configure the disturbance compensation input. In this case, a compensation input value can be generated by reconstructing the uncertainty estimated by the disturbance observer. Compensating for system uncertainty in this way is referred to as disturbance rejection control (DRC). DRC has been used in many transportation system applications to estimate and compensate for system uncertainty or external disturbances [23]–[25]. Fig. 1 shows a case in which DRC is applied to a DCT powertrain as a control scheme. In this figure, (x) is the feedback controller and (x) is the disturbance compensation gain. The plant of the control scheme consists of the DCT and the powertrain. The DCT model includes actuator nonlinearity to improve the control performance. In addition, the powertrain model can generally be expressed linearly. Therefore, DCT actuators in plants are classified as nonlinear and the powertrain is considered to be linear. Regarding the types of uncertainty in the DCT powertrain, there are the actuator uncertainty (d) and the road load torque (T_v). First, actuator uncertainty arises from a change in the friction coefficient or friction between components when measuring the actuator force. Because the actuator generates clutch torque, which is an input to the shift control system, this uncertainty is classified as a matched disturbance. Second, the road load torque, which is a type of disturbance in the powertrain, is generated in the drive torque, which is the output of the shift control system, as it includes changes in the drag force or road gradient, as well as the vehicle mass or inertia. However, it cannot be expressed as a matched disturbance by multiplying it by a transformation matrix. Therefore, it is a mismatched disturbance. These conditions are called matching conditions [26], [27].

That is, a DCT powertrain is a nonlinear system and is a system that includes a mismatched disturbance. Such a system can secure integrate stability if the composite control law is used. Therefore, the study of the composite control law for DRC was undertaken. First, a study of the composite control law assuming a matched disturbance in a nonlinear system was conducted [28]. Because this study deals with a matched disturbance, the disturbance compensation input can be constructed by multiplying the estimated disturbance by a matrix that transforms it into the input disturbance. A study applying a similar logic to position control of a surgical device was also conducted [29].

In a similar way to [28], a study to estimate the mis-

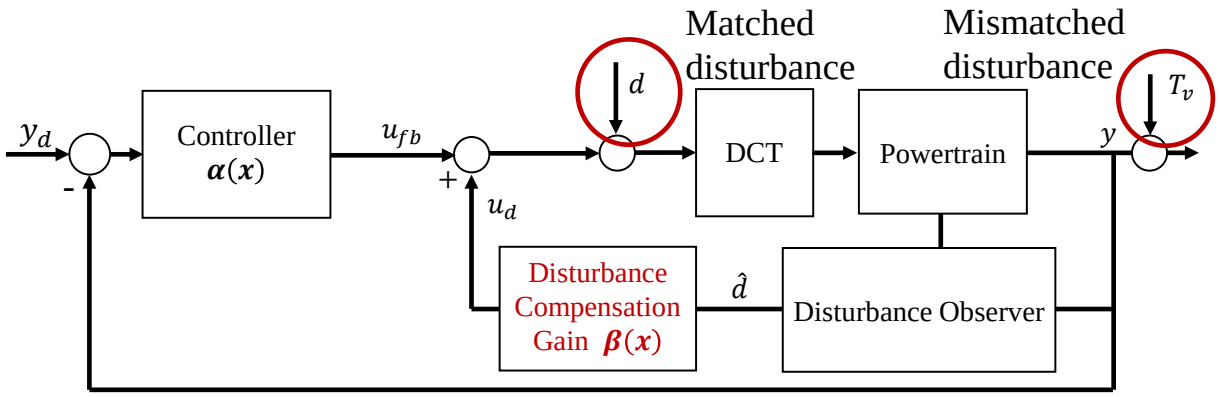

Figure 1. Disturbance configuration of the DCT powertrain model.

matched disturbance of a linearized nonlinear system was also conducted [30]. However, the limitations of linearization still exist. Furthermore, a study on the composite control law of a nonlinear system with mismatched disturbance without using linearization was also conducted [31]. In this study, the nonlinear functions of the target system are limited to the form in which the state is an argument. However, these studies cannot be applied to a DCT powertrain with nonlinearity. First, it has road load torque as a mismatched disturbance that is not transformed into an input disturbance. Second, it is a system in which the nonlinear functions of a system cannot take the form of an argument. Therefore, the composite control law as defined in existing studies cannot be used for DRC. A further analysis of the application of existing studies is presented in detail in Section III.

Therefore, in this paper, a composite control law for shift control of a DCT including nonlinearity is proposed, overcoming the shortcomings in existing studies. Therefore, the contribution of this paper is that it proposes a composite control law to reject a mismatched disturbance in a system with input nonlinearity, such as a DCT. The stability proof of the proposed method is also presented.

This paper deals with a DCT with input nonlinearity. In general, there is also a DCT with a change in the actuator lever ratio, but a BR-DCT using a self-energizing mechanism is selected as the target system here in order to consider a system with a large nonlinearity. In this system, the error of the actuator force sensor is uncertainty. At this time, uncertainty is estimated with the extended high-order disturbance observer (EH-DOB) presented in previous research [22]. The disturbance compensation input is then constructed using the composite control law proposed in this paper, combined with the input of the feedback controller, after which it is applied to the system. To verify the method proposed in this paper, a test bench simulating a powertrain equipped with a BR-DCT was constructed. Considering the limitations of the existing method, the validity of the proposed method is demonstrated through a shift experiment.

In Section II, the BR-DCT powertrain is modeled as the target system of this study. In this case, a BR-DCT actuator model with nonlinearity is used together. In Section III, the limitations are explained by examining the composite control law discussed in existing studies on the design of shift controllers, and a method to overcome these limitations is proposed. In Section IV, a shift controller using the proposed composite control law is designed using a feedback controller and a disturbance observer. In Section V, a shift experiment on the powertrain test bench is performed to verify the proposed method. Finally, this paper is concluded in Section VI.

II. System Modeling

A. Powertrain with DCT

To design a shift controller for DRC, a DCT powertrain must be modeled. At this time, for simplification of the system, lumped inertia is used without considering the inertia of each component individually; in the modeling of the DCT powertrain, two shift phases can be considered. Among them, in the torque phase (TP) in which the two clutch torques cross, a small average amount of torque is generated within a relatively short time, and the two clutch torques increase and decrease linearly, meaning that there is little decrease in the control performance due to uncertainty. Therefore, an open-loop control scheme is generally used in the torque phase. However, in the inertia phase (IP), which synchronizes the speed of the power source and the oncoming clutch, tracking control of the slip speed, which is the speed difference between the power source and the clutch, and drive torque for smooth synchronization are required. Estimation and rejection of uncertainty are important because the average clutch torque exceeds the TP and the reference composed of the smooth function must be tracked. Therefore, in this paper, we aim to improve the tracking control performance of the IP of the DCT powertrain. Here, for the IP, the torque of the offgoing clutch becomes 0. The input of the system becomes the torque of the power source and the torque of the oncoming clutch, and the output becomes the slip speed and the drive torque. In Fig. 2, the powertrain when upshifting is modeled. This model consists of a power source, a lumped clutch, and the vehicle inertia, and a compliance model was used for the drive shaft. The modeling referring to in this figure is as follows.

$$J_{ps}\,\dot{\omega}_{ps} = T_{ps} \quad T_{c1} \quad T_{c2} \tag{1}$$

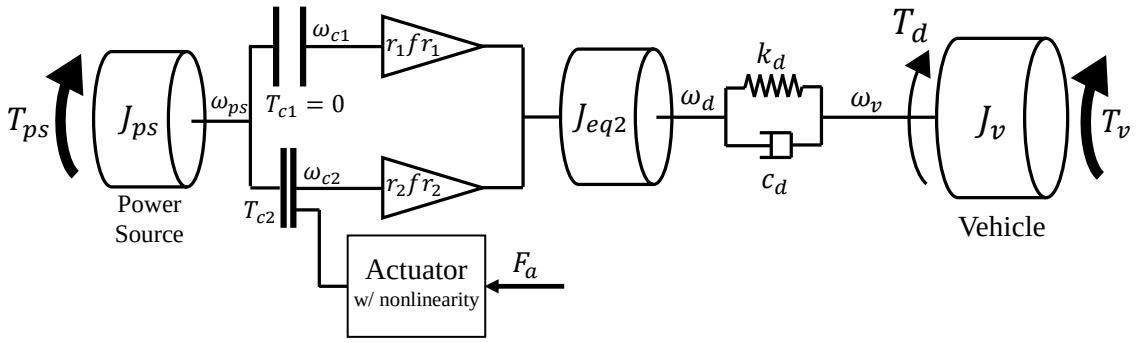

Figure 2. Modeling of a DCT powertrain with actuator nonlinearity.

$$J_{eq2}\frac{\dot{\omega}_{c2}}{r_2 r_{f2}} = r_2 r_{f2} T_{c2} \quad T_d \tag{2}$$

$$J_v \dot{\omega}_v = T_d \quad T_v = k_d(\quad_d \quad _v) + c_d(\omega_d \quad \omega_v) \quad T_v \tag{3}$$

Table I
DESCRIPTION OF POWERTRAIN MODEL NOTATIONS

Symbol	Name	Symbol	Name
J_{ps}	Power source inertia	J_{eq2}	Clutch 2 equivalent inertia
J_v	Vehicle inertia	ω_{ps}	Power source rotation speed
ω_{c2}	Clutch 2 rotation speed	ω_v	Wheel rotation speed
ω_d	Drive shaft rotation speed	$_d$	Drive shaft rotation angle
$_v$	Wheel rotation angle	T_{ps}	Power source torque
T_{c1}	Clutch 1 torque	T_{c2}	Clutch 2 torque
T_d	Drive shaft torque	T_v	Road load torque
r_1	First gear ratio	r_2	Second gear ratio
r_{f1}	First final gear ratio	r_{f2}	Second final gear ratio
k_d	Drive shaft stiffness	c_d	Drive shaft compliance

Notations for the expressions used here are indicated in Table. I. In this system, the inputs are the power source torque T_{ps} and the clutch 2 torque T_{c2}, and the outputs are the slip speed ω_{ps} ω_{c2} and the drive torque T_d. As mentioned in Section I, the road load torque T_v is a disturbance in the powertrain system.

B. Ball-ramp DCT

In this study, a system with both nonlinearity and uncertainty in the clutch actuator is targeted. Even in a general DCT actuator, nonlinearity and uncertainty exist due to a change in the lever ratio or friction among the parts. However, because the BR-DCT uses a self-energizing mechanism, various nonlinearities such as those associated with the lever ratio and the return spring angle arise [13], [14]. Moreover, because the sensor for measuring the force of the actuator is not installed inside the clutch pack, the error of the force sensor due to friction between the parts occurs as input uncertainty. Therefore, it can be seen as a system that requires more

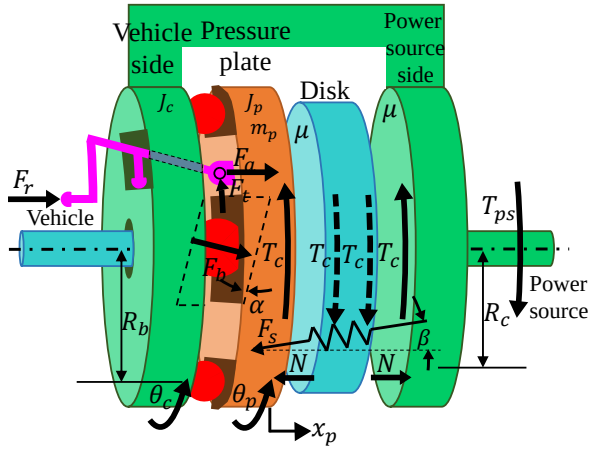

Figure 3. Free-body diagram of BR-DCT.

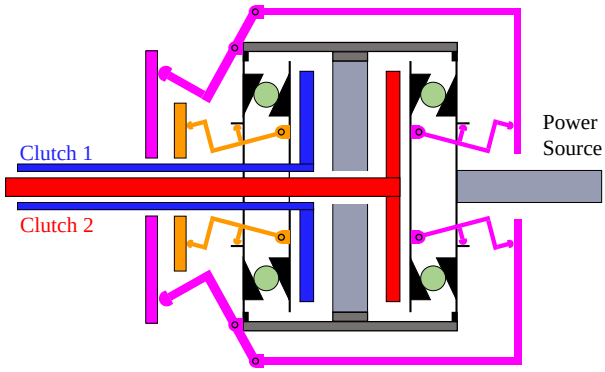

Figure 4. Cross-section of BR-DCT.

effective DRC. Therefore, the clutch pack and actuator of the BR-DCT can be modeled as shown in Fig. 3. This figure shows only the actuator mechanism of one clutch of BR-DCT. The entire mechanism of BR-DCT is shown in Fig. 4. The equilibrium equation derived from this modeling is as follows [22].

$$J_p \dot{\omega}_p = F_t R_a + T_c \quad F_b R_b \sin \quad F_s R_s \sin \tag{4}$$

$$m_p \ddot{x}_p = F_a + F_b \cos \quad F_s \cos \quad N \tag{5}$$

Table II
DESCRIPTION OF EACH NOTATIONS

Symbol	Name	Symbol	Name
N	Clutch disk Normal force		Clutch disk friction coefficient
$a; b$	Lever force moment arms	$a_f; b_f$	Lever friction force moment arms
$L(\ _{BR})$	Translation to rotation conversion ratio		Ramp angle
	Return spring angle	F_r	Release bearing force
F_a	Clutch actuator force	F_t	Clutch actuator rotational force
F_s	Return spring force	F_b	Ball reaction force
R_a	Lever actuation radius	R_b	Ball actuation radius
R_c	Clutch disk effective radius	R_s	Return spring actuation radius
T_c	Clutch friction torque	T_{ps}	Power source torque
$_p$	Pressure plate rotation angle	$_c$	Vehicle side plate rotation angle
$_{BR}$	Ball-ramp actuation angle	x_p	Pressure plate displacement
J_p	Pressure plate inertia	J_c	Vehicle side plate inertia
m_p	Pressure plate mass	m_c	Vehicle side plate mass

$$F_t = L(\ _{BR})F_a \tag{6}$$

$$T_c = \ NR_c \tag{7}$$

$$x_p = R_b\ _{BR}\tan \tag{8}$$

$$_{BR} = \ _p \quad _c \tag{9}$$

Here, (4), (5) and (6) are the torque, force and lever balance equations, respectively. In addition, (7) is the clutch friction torque equation and (8) and (9) are ball-ramp mechanism constraints. The notation of the parameters used here is indicated in Table II. Here, because the rigidity of both the pressure plate and ball is high, it is assumed that the deformation of these components is neglected. Also, it is assumed that N can be obtained using a pre-defined disk compression kinematics and via actuator encoder measurement. To derive $L(\ _{BR})$, the lever's FBD can be used, as shown in Fig. 5.

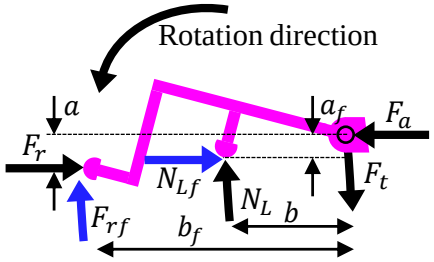

Figure 5. Free-body diagram of a self-energizing actuation lever.

As indicated in this figure, it can be assumed that the inertia term is negligible because the mass of the lever is very small. Therefore, the following equations can be derived.

$$F_a = \ 1 + \ _L\frac{_Lb_f \ \ a}{_La_f + b}\ F_r = T_r^a(\ _{BR})F_r \tag{10}$$

$$F_t = \frac{^2_La_f + a + \ _L(b \ \ b_f)}{^2_Lb_f + b + \ _L(a_f \ \ a)}F_a = L(\ _{BR})F_a \tag{11}$$

Where, F_r is the force exerted by the release bearing on the clutch actuator lever, and N_L is the rotational reaction force generated from the vehicle side plate. In addition, F_{rf} and N_{Lf} are frictional forces generated by F_L and N_L, respectively. $a; b; a_f$ and b_f are moment arms of $F_r; N_L; N_{Lf}$ and F_{rf}, respectively. Also, is the angle of the return spring. This value changes according to $_{BR}$, and it is assumed that it can be obtained using a pre-defined kinematics and actuator encoder. $_L$ is the coefficient of friction between the lever and vehicle side plate. Using the (10), F_a can be obtained from the release bearing force F_r. In addition, $L(\ _{BR})$ used in (6) can be obtained from (11).

Using the above equations, the clutch torque equation can be derived as follows.

$$T_c = \ R_c\frac{R_b\tan \ \ + LR_a}{R_b\tan \ \ \ R_c}F_a \\ R_c\frac{R_s\sin \ \ + R_b\tan \ \ \cos}{R_b\tan \ \ \ R_c}F_s \tag{12}$$

If (7) is applied to the left side of (12), the equation can be summarized as follows.

$$N = \frac{R_b\tan \ \ + LR_a}{R_b\tan \ \ \ R_c}F_a \\ \frac{R_s\sin \ \ + R_b\tan \ \ \cos}{R_b\tan \ \ \ R_c}F_s \tag{13}$$

In addition, (13) can be summarized for as follows.

$$= \frac{R_b\tan}{R_c} \quad \frac{(R_b\tan \ \ + LR_a)F_a}{R_cN} \\ \frac{(R_s\sin \ \ + R_b\tan \ \ \cos \ \ )F_s}{R_cN} \tag{14}$$

In (14), $L(\ _{BR}); \ ; F_s$ and N are variables determined by $_{BR}$. Therefore, (14) can be expressed as follows.

$$T_c = \ F_a(LR_a + R_b\tan \ \ ) \\ + F_s(R_s\sin \ \ + R_b\cos \ \ \tan \ \ ) \\ + R_bN\tan \tag{15}$$

C. BR-DCT powertrain with actuator nonlinearity

Equations (1), (2), (3) and (15) can be combined to form a system. At this time, the state consists of the slip speed, the compliance rate of the drive shaft and the drive torque. The powertrain model of the BR-DCT including actuator nonlinearity is as follows.

$$\underline{x} = f(x) + b_u(t)u + b_u(t)D \tag{16a}$$

$$y = Cx \tag{16b}$$

$$x = \begin{bmatrix} \omega_{ps} & \omega_{c2} \\ \frac{\omega_{c2}}{r_2 r_{f2}} & \omega_v \\ T_d & \end{bmatrix} \tag{17a}$$

$$f(x) = \begin{bmatrix} \frac{1}{J_{ps}} + \frac{(r_2 r_{f2})^2}{J_{eq2}} f_2(\theta_{BR}) + \frac{r_2 r_{f2}}{J_{eq2}} T_d \\ \frac{r_2 r_{f2}}{J_{eq2}} f_2(\theta_{BR}) - \left(\frac{1}{J_{eq2}} + \frac{1}{J_v}\right) T_d \\ \frac{c_d r_2 r_{f2}}{J_{eq2}} f_2(\theta_{BR}) + k_d \left(\frac{\omega_{c2}}{r_2 r_{f2}} - \omega_v\right) \\ c_d \left(\frac{1}{J_{eq2}} + \frac{1}{J_v}\right) T_d \end{bmatrix} \tag{17b}$$

$$b_u(t) = \begin{bmatrix} \frac{1}{J_{ps}} & -\frac{1}{J_{ps}} + \frac{(r_2 r_{f2})^2}{J_{eq2}} f_1(\theta_{BR}) \\ 0 & \frac{r_2 r_{f2}}{J_{eq2}} f_1(\theta_{BR}) \\ 0 & \frac{c_d r_2 r_{f2}}{J_{eq2}} f_1(\theta_{BR}) \end{bmatrix}; u = \begin{bmatrix} T_{ps} \\ F_a \end{bmatrix} \tag{17c}$$

$$b_d(t) = \begin{bmatrix} 0 & \frac{1}{J_{ps}} + \frac{(r_2 r_{f2})^2}{J_{eq2}} f_1(\theta_{BR}) \\ \frac{1}{J_v} & \frac{r_2 r_{f2}}{J_{eq2}} f_1(\theta_{BR}) \\ \frac{c_d}{J_v} & \frac{c_d r_2 r_{f2}}{J_{eq2}} f_1(\theta_{BR}) \end{bmatrix} \tag{17d}$$

$$D = \begin{bmatrix} T_v \\ d \end{bmatrix}; C = \begin{bmatrix} 1 & 0 & 0 \\ 0 & 0 & 1 \end{bmatrix} \tag{17e}$$

$$f_1(\theta_{BR}) = 2(LR_a + R_b \tan\theta) \tag{18}$$

$$f_2(\theta_{BR}) = 2F_s(R_s \sin\theta + R_b \cos\theta \tan\theta) + 2R_b N \tan\theta \tag{19}$$

III. Composite control law

A. Problem definition

For the DRC of the BR-DCT powertrain, a composite control law should be applied. To this end, we introduce the nomenclature used in existing studies. The matching condition mentioned in Section 1 can be expressed as follows.

$$Matching\ condition: b_u = \Gamma b_d \tag{20}$$

Here, Γ is a matrix that transforms the disturbance into the channel of the input. The target system for DRC can be configured as shown below.

$$\dot{x} = f(x) + b_u(x)u + b_d(x)d \tag{21}$$

$$u = \alpha(x) + \beta(x)\hat{d} \tag{22}$$

$$y = h(x) \tag{23}$$

Various studies have developed design methods of the disturbance compensation gain in relation to DRC in a nonlinear system. First, a study of the design of the compensation gain for a nonlinear system with a matched disturbance was performed [28]. In this case, it is assumed that $b_u(x)$ is invertible. The method of designing the compensation gain proposed in this study is as follows.

$$\beta(x) = -\frac{b_d(x)}{b_u(x)} \tag{24}$$

The composite control law u using (24) can be expressed as follows. Here, because it is assumed that only a matched disturbance exists, (22) can be summarized using the matching condition of (20).

$$u = \alpha(x) - \hat{d} \tag{25}$$

In this study, the stability of the composite control law designed using (25) was verified through a Lyapunov stability analysis. In conclusion, by designing a composite controller using (25) and the feedback controller $\alpha(x)$ designed under the assumption that there is no disturbance in the plant, it was proved that the tracking error and the disturbance estimation error can converge to zero. That is, it has been proved that DRC is possible. However, this is limited to systems with only matched disturbances.

To address this problem, a study was conducted to control disturbance compensation by extending the system with a mismatched disturbance [31]. In this study, DRC was performed for the following systems.

$$\dot{x} = f(x)x + b_u(x)u + b_d(x)d \tag{26a}$$

$$u = \alpha(x)x + \beta(x)\hat{d} \tag{26b}$$

$$y = h(x)x \tag{26c}$$

The method of designing the compensation gain proposed in this study is as follows. At this time, it is assumed that $b_u(x)$ is invertible and the system has a mismatched disturbance ($b_d \neq b_u$).

$$\beta(x) = -h(x)[f(x) + b_u(x)\alpha(x)]^{-1} b_u(x)^{-1} h(x)[f(x) + b_u(x)\alpha(x)]^{-1} b_d(x) \tag{27}$$

Also, a Lyapunov stability analysis serves to determine the stability of a system to which a composite control law designed using (27) is applied. However, this is limited to the system expressed as (26). Therefore, the aforementioned studies cannot be used for shift control of a BR-DCT. First, the method suggested by [28] cannot be used because the system has both matched and mismatched disturbances. Also, referring to (16) and (17), the method proposed by [31] cannot be used because the BR-DCT powertrain system cannot be expressed as a system such as (26). Additionally, $b_u(t)$ is not invertible. The existence of the inverse matrix of $b_u(t)$ indicates the state-input condition of the system. That is, the number of inputs and states is the same, and the input affects all states independently. However, in BR-DCT, there is no

inverse matrix of $b_u(t)$ because there are more states than inputs. Therefore, it is necessary to design a composite control law applicable to the BR-DCT powertrain system. In this paper, a modified composite control law based on the previous research was proposed for the BR-DCT powertrain system.

B. Proposed composite control law

In order to design a modified composite control law based on previous research, it is necessary to understand the characteristics of the target system. The BR-DCT powertrain system is represented by (16), where $b_u(t)$ is not invertible but $Cb_u(t)$ is invertible. That is, it can be expressed as $y \ 2 <^m; u \ 2 <^m$, which means that the numbers of y and u are identical. There is also the condition $b_u(t) \ 6= \ b_d(t)$ for mismatched disturbances. Therefore, the generalization of the BR-DCT powertrain system proceeds as follows.

$$\underline{x} = f(x) + b_u(t)u + b_d(t)d \tag{28a}$$
$$y = Cx \tag{28b}$$

A composite control law that guarantees the integrated stability of a system with these conditions can be proposed as shown below.

Theorem 1. *Consider a nonlinear system with a mismatched disturbance as* (28)*. The closed-loop system under a nonlinear composite controller designed by the following procedure is semi-globally exponentially stable in the sense that for an initial state x and e_d satisfying:*

$$kx(0)k \quad v_1; ke_d(0)k \quad v_2 \tag{29}$$

where v_1 and v_2 are the given scalars (which may be arbitrarily large).

1) *Design a controller for system to obtain stability and other performance specifications under the assumption that the disturbance is measurable and the following Lyapunov candidate function is a positive definite.*

$$V_c(x) = x^T C^T Cx \tag{30}$$

2) *Construct a disturbance observer to estimate the disturbance under the following Lyapunov candidate function as positive definite.*

$$V_o(e_d) = e_d^T P e_d \tag{31}$$

where, $P > 0$ is symmetric matrix.

3) *Integrate the disturbance observer with the controller if the disturbance compensation gain (x) is selected such that the following condition holds:*

$$(x) = \quad Cb_u(t) \quad {}^1 Cb_d(t) \tag{32}$$

Proof. As defined in (22), the composite control input $u = (x) + (x)\hat{d}$ consists of a feedback controller and a disturbance compensation input. It is expressed as follows by combining the composite control law and the target plant of the (28).

$$\underline{x} = f(x) + b_u(t) \ (x) \quad b_u(t) \ (x)e_d + b_d(t) + b_u(t) \ (x) \ d \tag{33}$$

Multiplying both sides of (33) by C gives the following result.

$$C\underline{x} = C \ f(x) + b_u(t) \ (x) \quad Cb_u(t) \ (x)e_d + Cb_d(t) + Cb_u(t) \ (x) \ d \tag{34}$$

Here, substituting the disturbance compensation gain (x) defined from (32) is as follows.

$$C\underline{x} = C \ f(x) + b_u(t) \ (x) \quad Cb_u(t) \ (x)e_d \tag{35}$$

In addition, the Lyapunov candidate function $V_c(x)$ of the designed controller and its derivative can be obtained through *procedure* 1.

$$V_c(x) = x^T C^T Cx \tag{36a}$$
$$\dot{V}_c(x) = 2x^T C^T C\underline{x} = 2x^T C^T C \ f(x) + b_u(t) \ (x) \tag{36b}$$
$$< \quad {}_1 kxk \tag{36c}$$

where $_1$ is a small positive scalar. As above, using *procedure* 1 proves that $\dot{V}_c(x)$ is negative definite.

Subsequently, the Lyapunov candidate function $V_o(e_d)$ of the nonlinear DOB is designed through *procedure* 2 and its derivative can be obtained.

$$V_o(e_d) = e_d^T P e_d \tag{37a}$$
$$\dot{V}_o(e_d) = 2e_d^T P \underline{e}_d < \quad {}_2 kxk \tag{37b}$$

where $_2$ is a small positive scalar. Similarly, using *procedure* 2 proves that $\dot{V}_o(e_d)$ is negative definite.

In order to verify the integrated stability of the system to which the composite control is applied, the integrated Lyapunov candidate function can be obtained as follows.

$$V(x; e_d) = \ {}_1 V_c(x) + \ {}_2 V_o(e_d) \tag{38a}$$
$$= \ {}_1 x^T C^T Cx + \ {}_2 e_d^T P e_d \tag{38b}$$

Here, the derivative of $V(x; e_d)$ is as follows.

$$\dot{V}(x; e_d) = 2 \ {}_1 x^T C^T C\underline{x} + 2 \ {}_2 e_d^T P \underline{e}_d \tag{39}$$

where $_1$ and $_2$ are a positive scalar. When summarized by substituting (35) for (39), it proceeds as follows.

$$\dot{V}(x; e_d) = 2 \ {}_1 x^T C^T \Big\{ C \ f(x) + b_u(t) \ (x) + Cb_d(t)e_d \Big\} + 2 \ {}_2 e_d^T P \underline{e}_d \tag{40}$$

$$\dot{V}(x; e_d) < \quad {}_1 \ {}_1 kxk + 2 \ {}_1 x^T Cb_d(t)e_d \quad {}_2 \ {}_2 ke_d k \tag{41}$$

It is concluded that all states and observer errors starting from a possible arbitrarily large set converge to the origin as $t \ ! \ 1$. □

IV. Shift controller design for BR-DCT with the proposed composite control law

To apply the modified control law presented in Section III to the shift control of a BR-DCT, the procedures of *Theorem* 1 were applied.

A. Design a controller with $V_c(x) = x^T C^T C x$

The *procedure* 1 requires the selection of an appropriate feedback controller. The controller should be designed using $V_c(x) = x^T C^T C x$, but there is no need to use a nonlinear system as the target system as a nonlinear disturbance observer. For the nonlinear disturbance observer, because the uncertainty of F_a was estimated, the actuator kinematics with nonlinearity was used. However, the feedback controller can use T_{c2} as input and convert this value to F_a using actuator kinematics, meaning that the controller can use only a powertrain model without actuator kinematics. Here, the powertrain model is a linear system and therefore a linear controller can be used. The powertrain model used in the controller design is as follows.

$$\dot{x} = Ax + Bu + ET_v \tag{42a}$$
$$y = Cx \tag{42b}$$

$$x = \begin{bmatrix} \omega_{ps} \\ \omega_{c2} \\ \frac{\omega_{c2}}{r_2 r_{f2}} \\ T_d \end{bmatrix}; A = \begin{bmatrix} 0 & 0 & \frac{r_2 r_{f2}}{J_{eq2}} \\ 0 & 0 & \frac{1}{J_{eq2}} + \frac{1}{J_v} \\ 0 & k_d & c_d \end{bmatrix}; \frac{1}{J_{eq2}} + \frac{1}{J_v}$$

$$B = \begin{bmatrix} \frac{1}{J_{ps}} & \frac{1}{J_{ps}} + \frac{(r_2 r_{f2})^2}{J_{eq2}} \\ 0 & \frac{r_2 r_{f2}}{J_{eq2}} \\ 0 & \frac{c_d r_2 r_{f2}}{J_{eq2}} \end{bmatrix}; u = \begin{bmatrix} T_{ps} \\ T_{c2} \end{bmatrix};$$

$$E = \begin{bmatrix} 0 \\ \frac{1}{J_v} \\ \frac{c_d}{J_v} \end{bmatrix}; C = \begin{bmatrix} 1 & 0 & 0 \\ 0 & 0 & 1 \end{bmatrix} \tag{43}$$

Also, $V_c(x) = x^T C^T C x$ can be expressed as $V_c(x) = y^T y$ using $y = Cx$. Therefore, it becomes a problem to design a controller that stabilizes y.

Because the DOB is used for disturbance compensation in the shift controller of the BR-DCT, the DOB acts as an inner-loop controller undertaking control following the plant model used in the design. Therefore, it is necessary to select a controller that can utilize these characteristics. In other words, a robust controller should be selected such that the more accurate the plant model used is, the more robust the control becomes. In this case, even if there is a difference between the actual model and the nominal model, robustness can be secured by compensating for disturbances. Accordingly, this strategy is suitable for a system with a considerable amount of friction caused by mechanical parts or many changes in plant parameters. Also, the BR-DCT powertrain system has many mechanical components, and plant parameters such as the clutch touchpoint or thickness of the clutch disk may change. Therefore, shift controllers should utilize a model-based controller that ensures robustness. In this study, a H_1 loop-shaping controller [32], [33] was used as a feedback controller. Although in this paper, a H_1 loop-shaping controller is used as a controller, a range of other types of controllers can be applied depending on the characteristics or environments of the plant. The H_1 loop-shaping controller used in this paper is one of those examples.

The objective of the H_1 loop-shaping controller is to design pre-compensator $W(s)$ and feedback controller $K_1(s)$ that satisfies the following condition:

$$G_s(s) = W(s)G(s) \quad ! \quad G_d(s) \tag{44}$$

$$\begin{aligned} &\_(G_s K_1) \quad \frac{1}{-}\_(G_d); \quad (G_s K_1) \qquad (G_d) \\ &\text{and maximize} \quad = \frac{W(s)}{} \end{aligned} \tag{45}$$

Here, $\_(\ )$ represents the minimum singular value, $(\ )$ represents the maximum singular value, and represents the boundary where $K_1(s)G_s(s)$ exists based on $G_d(s)$. That is, it represents the range in which a controlled plant can exist according to the maximum value of uncertainty. Because the size of this boundary is determined according to the shape of $G_d(s)$, using (45), $K_1(s)$ is feasible with the following equation.

$$= \min_{K_\infty} \quad \begin{matrix} I \\ K_1 \end{matrix} \quad (I \quad G_s K_1)^{\ 1} \ G_s \quad I \qquad _{H_\infty} \tag{46}$$

When designing a H_1 loop-shaping controller via the method described above, the maximum permissible difference between a nominal shaped plant and a perturbed shaped plant is determined in . Reducing differences in perturbed plants through sophisticated modeling of nominal plants can allow for greater tolerance for uncertainty due to unexpected plant parameter changes. From this point of view, a disturbance-compensated plant can be viewed as reducing the difference between a nominal plant and a perturbed plant using DOB. That is, if there is a disturbance-compensation inner loop, as shown in the Fig. 6, the system including the inner loop can be considered as a lumped plant defined by G_{DOB}. At this time, G_{DOB} follows the nominal plant $G(s)$ used in the DOB design due to inner loop compensation. In other words, from the perspective of the H_1 loop-shaping controller, the accuracy of the nominal plant increases, thus reducing the difference from the perturbed plant and increasing the uncertainty boundary. In conclusion, it is possible to increase the relative uncertainty bounds of model-based robust controllers such as H_1 loop-shaping controllers in systems with a disturbance-compensating inner loop.

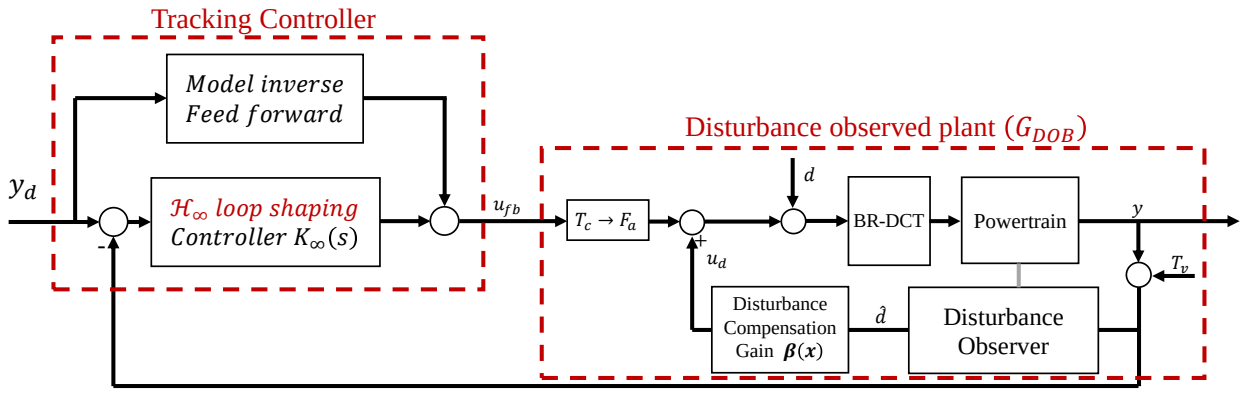

Figure 6. Schematic diagram of the BR-DCT powertrain system using the H_1 loop-shaping controller and EH-DOB.

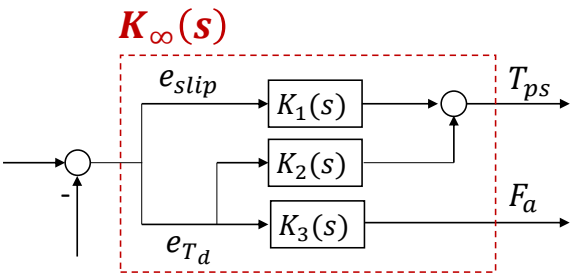

Figure 7. H_1 loop-shaping controller $K_1(s)$ designed using *procedure* 1.

Table III
DESCRIPTION OF POWERTRAIN PARAMETERS

Symbol	Name
J_{ps}	$0.22kg\ m^2$
J_{eq2}	$17.65kg\ m^2$
r_1	3.85
r_2	2
r_{f1}	4
r_{f2}	4.17

The H_1 loop-shaping controller was designed as shown in Fig. 7 for shift control of the BR-DCT powertrain. Here, each internal controller is as follows.

$$K_1(s) = \frac{1.18s^2 + 100s + 0.05}{0.16s^2 + 12.9s + 0.003}$$
$$K_2(s) = \frac{0.18s^3 + 1.18s^2 + 100s + 0.02}{0.30s^3 + 28.0s^2 + 0.006s} \quad (47)$$
$$K_3(s) = \frac{0.007s^3 + 1.18s^2 + 100s + 0.02}{0.34s^2 + 28.0s^2 + 0.007s}$$

The parameters of the powertrain model used here are given in Table III.

B. Construct a disturbance observer with $V_o(x) = e_d^T P e_d$

Because the design of the feedback controller was completed in Subsection IV-A, the nonlinear DOB should be designed according to *procedure* 2. When designing this using $V_o(x) = e_d^T P e_d$, if $P = \begin{matrix} 1 & 0 \\ 0 & 1 \end{matrix}$, $V_o(x)$ becomes $V_o(x) = e_d^T e_d$, which becomes a problem when designing a disturbance observer that converges e_d to zero. In this paper, an EH-DOB designed in previous work is used [22]. To estimate the uncertainty of the BR-DCT system using the EH-DOB, the generalization of the BR-DCT powertrain system using (16) proceeds as follows.

$$\dot{x} = f_{BR}(x;u;t) + F_{BR}(t)D \quad (48)$$

$$f_{BR}(x;u;t) = f(x) + b_u(t)u \quad (49a)$$
$$F_{BR}(t) = b_d(t) \quad (49b)$$

Here, $x = \begin{matrix} 2 & \omega_{ps} & \omega_{c2} & 3 \\ 6 & \omega_{c2} & & 7 \\ 4 & \overline{r_2 r_{f2}} & \omega_v & 5 \\ & T_d & & \end{matrix}$ is the state vector of the system, and $D = \begin{matrix} d \\ T_v \end{matrix}$ is the uncertainty of the BR-DCT powertrain system.

In this case, it is assumed that the disturbance of the BR-DCT is expressed as a polynomial with respect to time, as follows.

$$d(t) = \sum_{k=0}^{N} d_i t^k \quad (50)$$

The EH-DOB as proposed in previous research can be applied to estimate the uncertainties in the system, as follows using (48).

$$\dot{z} = F_{BR}^{+}(t)x + F_{BR}^{+}(t)f_{BR}(x;u;t) + \dot{\hat{D}} \quad (51a)$$
$$\dot{\hat{D}} = \sum_{k=0}^{N} {}_k g_k(t) \quad (51b)$$

$$g_k(t) = \begin{cases} F_{BR}^{+}(t)x - z; & (k=0) \\ \int_0^t g_{k-1} d\tau; & (k \geq 1) \end{cases} \quad (52)$$

The EH-DOB of the BR-DCT designed by the proposed method uses the powertrain parameters in Table III. In addition, the maximum order of disturbance and the position

Table IV
DESCRIPTION OF EH-DOB PARAMETERS

Symbol	Name
$n(d^{(n)} = 0)$	3
q	3
$p1$	-10
$p2$	-10
$p2$	-10

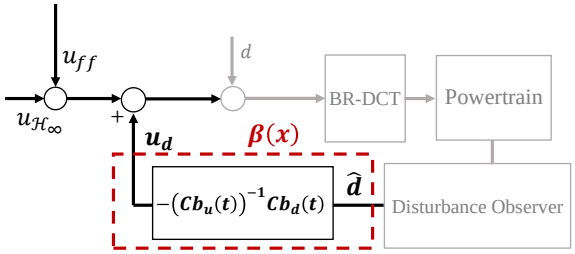

Figure 8. Disturbance compensation gain (x) designed using *procedure* 3.

of each pole in Table IV were specified through an actual disturbance analysis. Considering that the third derivative value converges to 0, n and q are set to 3.

To investigate the convergence of the error dynamics of the proposed EH-DOB, the disturbance estimation error $e_d = \hat{d}\ \ d$ can be written as follows.

$$e_d = z \quad F^+(t)x \quad F^+(t)x \tag{53}$$

The $(q+1)$-th derivative of (53) is as follows.

$$e_d^{(q+1)} + \ {}_0e_d^{(q)} + \quad + \ {}_qe_d = d^{(q+1)} \tag{54}$$

Here, $(\ )^{(k)}$ is the k-th derivative of the function. According to the disturbance information in the (50), $d^{(q+1)} = 0$. Therefore, the j-th row of the Laplace transform of (54) is expressed as follows.

$$E_{dj}(s)(s^{q+1} + \ {}_{0j}s^q + \quad + \ {}_{(q\ \ 1)j}s + \ {}_{qj}) = 0 \tag{55}$$

The characteristic equation of error dynamics can be obtained through (55). Because of all the poles of the characteristic equation are in the LHP, the error dynamics of H-DOB are asymptotically and exponentially stable against the initial error. Therefore, it is proved that $V_o(x) = 2e_d^T e_d < 0$.

C. Integrate the disturbance observer with the controller

As the designs of the feedback controller and DOB in Subsection IV-A and Subsection IV-B are complete, use the disturbance compensation gain of (32) to integrate the DOB and feedback controller according to *procedure* 3, as shown in Fig. 8.

V. EXPERIMENTAL VERIFICATION OF THE PROPOSED COMPOSITE CONTROL LAW

A. Experimental setup

To verify the proposed composite control law, a test bench that simulates the vehicle's powertrain was designed. All parts are manufactured as modules and can be exchanged according to the type of experiment.

The test bench consists of a power source, the DCT, a vehicle, and a load module. A permanent-magnet synchronous motor (PMSM) was used as the power source module connected to the rotational inertia, and the BR-DCT module was composed of a clutch pack and actuators, gears, torque sensors for verification, and final gears. In order to reduce the complexity of the system, each shaft on which a torque sensor is installed is fixed to the first and second gears.

The vehicle module is composed of a shaft to ensure compliance so as to realize the vibration of the drive shaft, along with a disk plate and reduction gear to implement the body mass. The vehicle module used in the test bench was designed to target 1500kg, which is the weight of a typical passenger car. The load module is designed to generate load torque using an electro-hydraulic brake system.

The performance of the shift controller is verified through a shift experiment using the composite control law designed in Section IV. To verify the performance of the controller, an experiment using an acceleration shift scenario was selected. In this verification experiment, the experimental scenario of shifting from first gear to second gear was used.

B. Experiment results

To compare the performance of the DRC proposed in this paper, the results of the proposed DRC experiment were compared with the results when using the conventional composite control law [28]. At this time, the H_1 loop-shaping controller designed in Subsection IV-A and the EH-DOB designed in Subsection IV-B were commonly used for a fair comparison. The BR-DCT powertrain test bench used as the experimental equipment is shown in Fig. 9. In both experiments, the same amount of power source torque was applied and a scenario in which shifting at $300rpm$ took place was selected. Also, the reference of the slip speed and drive torque in IP is set to be identical. The results of the shift control performance comparison experiment under these conditions are shown in Figs. 10 and 11.

Fig. 10 is the experimental result when the conventional composite control law is used. In this experiment, acceleration was performed while maintaining the power source torque at $16Nm$ with the first gear engaged. As shown in Fig. 10, when the speed of clutch 1 reaches $300rpm$, the shift controller that receives the shift command performs TP control for about 0.5 seconds and IP control for about 0.8 seconds. TP starts at 12.4 seconds and IP starts at 13.05 seconds. Because this experiment uses the conventional composite control law, the stability of controller is not guaranteed. Therefore, despite the fact that the disturbances are appropriately estimated in (c) and (f) in Fig. 10, the control performance is poor. Indeed, the controlled outputs, i.e., the slip speed and the drive torque, diverged.

Fig. 11 shows the experimental results when a robust controller with the proposed composite control law is used. Also in this experiment, while the first gear is engaged, the power source torque is maintained at $17Nm$ under acceleration.

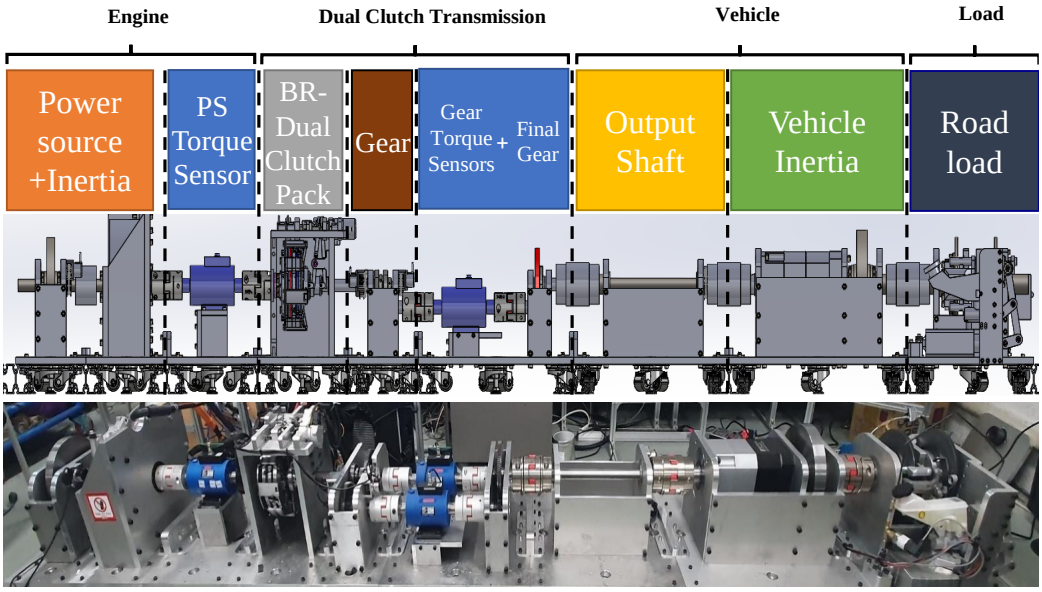

Figure 9. The test bench that simulates the powertrain of a vehicle is equipped with a BR-DCT. It is also equipped with a torque sensor for verification that can measure the torque of the power source and clutch. Each part is designed as a module and can be replaced.

When the speed of the clutch 1 reaches $300rpm$, the shift controller that receives the shift command performs TP control for about 0.5 seconds and IP control for about 0.8 seconds. As shown in Fig. 11, TP starts at 4.6 seconds and IP starts at 5.2 seconds. Identical to Fig. 10, the uncertainty of the actuator model is well estimated, as shown in (c) and (f) of Fig. 11. Because the composite control law, which integrates stability, is guaranteed, the DRC can work effectively. As a result, the tracking control performance of the slip speed and drive torque is improved. Specifically, the RMS value of the slip speed tracking error was $0.33rad/s$ and the RMS value of the drive torque tracking error was $8.00Nm$. Moreover, the RMS of the estimation error after the convergence of the disturbance is $15.13N$ for d and $24.83Nm$ for T_v, which is very low compared to the average value. In addition, accurate shift timing was secured with the planned shift time. In conclusion, it was verified that the disturbance rejection shift control of the BR-DCT with the proposed composite control law showed better shift control performance than the conventional composite control law.

Fig. 12 shows the sensitivity function between the disturbances and the tracking errors. This figure presents the performance of the disturbance rejection as a sensitivity function. If the magnitude of the sensitivity function is lower than zero, disturbance rejection is suitably performed. In Fig. 12, all of the magnitude of the sensitivity function between the slip speed tracking error e_1, the drive torque tracking error e_2 and actuator uncertainty d, and the road load torque T_v is less than zero at every frequency. That is, the shift controller of the BR-DCT using the proposed control law and an EH-DOB shows robust control performance.

VI. Conclusion and Future Work

In Section IV, a composite control law using an EH-DOB and a tracking controller is designed for disturbance rejection shift control of a BR-DCT. For this purpose, previous studies of nonlinear DOB-based control schemes were investigated, but these studies could not be applied to the BR-DCT powertrain system. In particular, because the BR-DCT powertrain system includes not only matched disturbances but also mismatched disturbances, it was difficult to apply the findings in previous studies when they dealt only with matched disturbances. In addition, the BR-DCT powertrain system did not satisfy the target system conditions of previous studies dealing with mismatched disturbances. Therefore, in this paper, a modified composite control law was proposed. The proposed composite control law is suitable for application to systems represented by the BR-DCT powertrain system. The closed-loop stability of the proposed composite control law was verified through a Lyapunov stability analysis.

Then, the shift controller of the BR-DCT was designed using the proposed composite control law. A H_1 loop-shaping controller was used as a feedback controller to maximize the characteristics of the disturbance compensation system and an EH-DOB was used as a disturbance observer. Finally, integrated stability was verified by applying the disturbance compensation gain of the proposed composite control law. To verify the proposed shift controller, a shift control experiment using a BR-DCT test bench was conducted. For comparison, experiments were also performed when the conventional composite control law was used. As a result of the verification experiment, the result of the DRC using the proposed composite control law guaranteed integrated stability and minimized the RMS value of the tracking error compared to when the conventional composite control law was used. In conclusion, it was verified that the shift control performance of the proposed

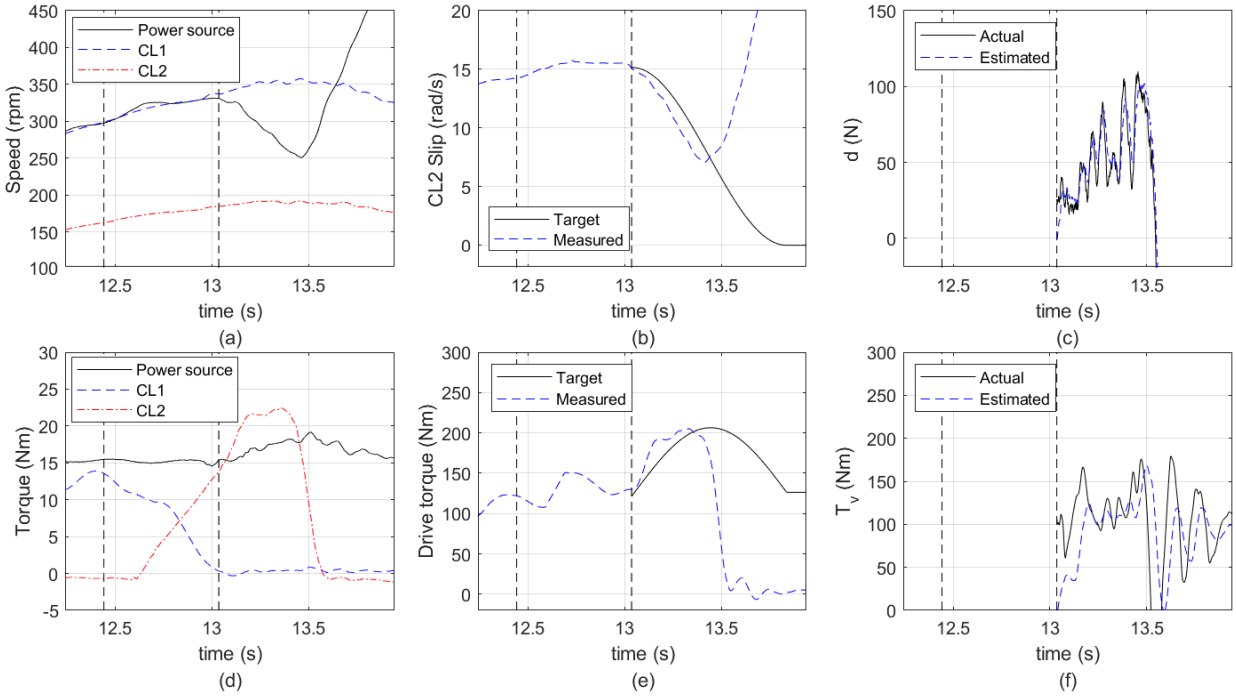

Figure 10. Result of the acceleration up-shift experiment using the conventional composite control law with the H_1 loop-shaping controller and an EH-DOB.

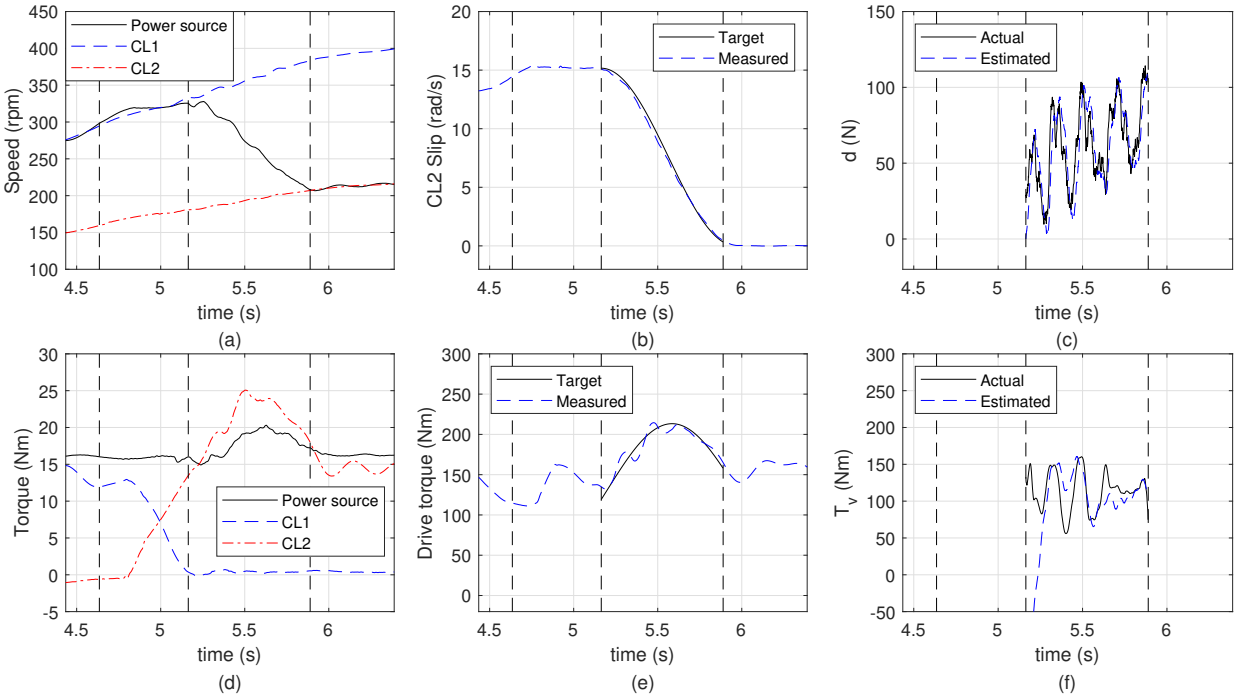

Figure 11. Result of the acceleration up-shift experiment using the proposed composite control law with the H_1 loop-shaping controller and an EH-DOB.

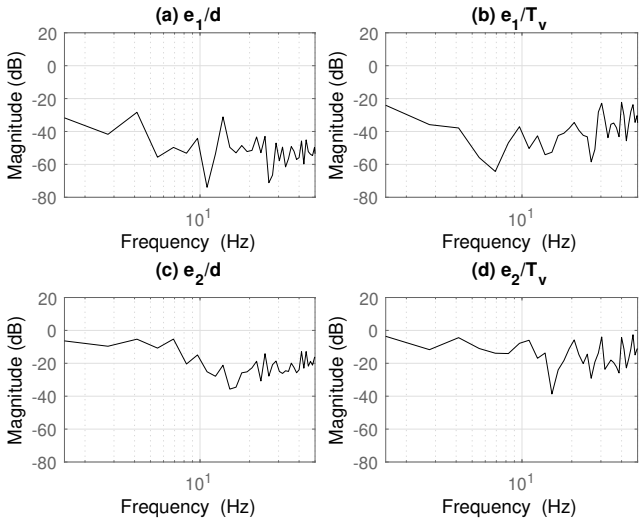

Figure 12. Magnitude of the sensitivity function between the disturbances and tracking errors to verify the performance of the disturbance rejection.

BR-DCT with the DRC is superior to the case where the conventional composite control law was used.

In this paper, a power-on up-shift scenario was selected as an experiment to verify the proposed composite control law. However, it is necessary to verify the proposed algorithm with a scenario assuming various shift situations, such as power-on down-shift. Additionally, in the proposed method, the DOB and controller were designed separately. That is, when designing the controller, it is assumed that there is no disturbance, and when designing the DOB, control input is not considered. However, each input from the DOB and controller is applied to a single system. Therefore, it is necessary to consider both in mutual designs. These complementary design methods will be addressed in further studies.

ACKNOWLEDGMENTS

This work was supported by the National Research Foundation of Korea(NRF) grant funded by the Korea government(MSIP) (No. 2020R1A2B5B01001531), the Technology Innovation Program (20014983, Development of autonomous chassis platform for a modular vehicle) funded By the Ministry of Trade, Industry & Energy(MOTIE, Korea), and the BK21+ program through the NRF funded by the Ministry of Education of Korea.

REFERENCES

[1] Z. Zhao, Z. Wei, G. Wu, and M. J. Barth, "Developing a data-driven modularized model of a plug-in hybrid electric bus (pheb) for connected and automated vehicle applications," in *2020 IEEE 23rd International Conference on Intelligent Transportation Systems (ITSC)*. IEEE, 2020, pp. 1–6.

[2] S. Cheng, L. Li, X. Chen, S.-n. Fang, X.-y. Wang, X.-h. Wu, and W.-b. Li, "Longitudinal autonomous driving based on game theory for intelligent hybrid electric vehicles with connectivity," *Applied energy*, vol. 268, p. 115030, 2020.

[3] S. A. Bonab and A. Emadi, "Mpc-based energy management strategy for an autonomous hybrid electric vehicle," *IEEE Open Journal of Industry Applications*, vol. 1, pp. 171–180, 2020.

[4] H. Kuroiwa, N. Ozaki, T. Okada, and M. Yamasaki, "Next-generation fuel-efficient automated manual transmission," *Hitachi Review*, vol. 53, no. 4, pp. 205–209, 2004.

[5] J. Franco, M. A. Franchek, and K. Grigoriadis, "Real-time brake torque estimation for internal combustion engines," *Mechanical Systems and Signal Processing*, vol. 22, no. 2, pp. 338–361, 2008.

[6] G. Lucente, M. Montanari, and C. Rossi, "Modelling of an automated manual transmission system," *Mechatronics*, vol. 17, no. 2-3, pp. 73–91, 2007.

[7] B. Mashadi, A. Kazemkhani, and R. B. Lakeh, "An automatic gear-shifting strategy for manual transmissions," *Proceedings of the Institution of Mechanical Engineers, Part I: Journal of Systems and Control Engineering*, vol. 221, no. 5, pp. 757–768, 2007.

[8] S. I.-N. Delhi, "Automatic transmissions—amt takes on at, cvt, dct," *Auto Tech Review*, vol. 12, no. 5, pp. 20–23, 2016.

[9] C. H. F. Amendola and M. A. L. Alves, "Gear shift strategies analysis of the automatic transmission in comparison with the double clutch transmission," SAE Technical Paper, Tech. Rep., 2006.

[10] H. Chen and B. Gao, *Nonlinear estimation and control of automotive drivetrains*. Springer Science & Business Media, 2013.

[11] H. Faust, C. Bünder, and E. DeVincent, "Dual clutch transmission with dry clutch and electro-mechanical actuation," *ATZautotechnology*, vol. 10, no. 2, pp. 32–37, 2010.

[12] J. Kim and S. B. Choi, "Design and modeling of a clutch actuator system with self-energizing mechanism," *IEEE/ASME Transactions on Mechatronics*, vol. 16, no. 5, pp. 953–966, 2010.

[13] D.-H. Kim, J.-W. Kim, and S. B. Choi, "Design and modeling of energy efficient dual clutch transmission with ball-ramp self-energizing mechanism," *IEEE Transactions on Vehicular Technology*, vol. 69, no. 3, pp. 2525–2536, 2019.

[14] D.-H. Kim and S. B. Choi, "Design of ball-ramp dual clutch transmission to reduce uncertainties in clutch actuator and tie-up effect," *Mechanism and Machine Theory*, vol. 176, p. 104982, 2022.

[15] B. Matthes, "Dual clutch transmissions–lessons learned and future potential," *SAE transactions*, pp. 941–952, 2005.

[16] C.-Y. Cho, J.-H. Kam, H.-K. Hong, and C. Lövenich, "More efficiency with the dry seven-speed dual-clutch transmission by hyundai," *ATZ worldwide*, vol. 118, no. 6, pp. 38–41, 2016.

[17] J. Deur, M. Milutinović, V. Ivanović, and H. Eric Tseng, "Modeling of a dry dual clutch utilizing a lever-based electromechanical actuator," *Journal of dynamic systems, measurement, and control*, vol. 138, no. 9, p. 091012, 2016.

[18] Z. Zhao, X. Li, L. He, C. Wu, and J. K. Hedrick, "Estimation of torques transmitted by twin-clutch of dry dual-clutch transmission during vehicle's launching process," *IEEE transactions on vehicular technology*, vol. 66, no. 6, pp. 4727–4741, 2016.

[19] J. J. Oh, J. S. Eo, and S. B. Choi, "Torque observer-based control of self-energizing clutch actuator for dual clutch transmission," *IEEE Transactions on Control Systems Technology*, vol. 25, no. 5, pp. 1856–1864, 2016.

[20] J. J. Oh and S. B. Choi, "Real-time estimation of transmitted torque on each clutch for ground vehicles with dual clutch transmission," *IEEE/ASME Transactions on Mechatronics*, vol. 20, no. 1, pp. 24–36, 2014.

[21] J. Kim, J. Oh, and S. B. Choi, "Nonlinear estimation method of a self-energizing clutch actuator load," in *2012 First International Conference on Innovative Engineering Systems*. IEEE, 2012, pp. 231–236.

[22] D.-H. Kim and S. B. Choi, "Extended high-order disturbance observer-based clutch actuator model uncertainty estimation of ball-ramp dual-clutch transmission," *IEEE Transactions on Control Systems Technology*, 2022.

[23] X. Wang, L. Zhu, H. Wang, T. Tang, and K. Li, "Robust distributed cruise control of multiple high-speed trains based on disturbance observer," *IEEE Transactions on Intelligent Transportation Systems*, no. 1, pp. 267–279, 2019.

[24] C. Tang, Z. Xu, and M. Tomizuka, "Disturbance-observer-based tracking controller for neural network driving policy transfer," *IEEE Transactions on Intelligent Transportation Systems*, no. 9, pp. 3961–3972, 2019.

[25] X. Hu, X. Wei, Y. Kao, and J. Han, "Robust synchronization for under-actuated vessels based on disturbance observer," *IEEE Transactions on Intelligent Transportation Systems*, no. 6, pp. 5470–5479, 2021.

[26] S. Li, J. Yang, W.-H. Chen, and X. Chen, *Disturbance observer-based control: methods and applications*. CRC press, 2014.

[27] W.-H. Chen, J. Yang, L. Guo, and S. Li, "Disturbance-observer-based control and related methods—an overview," *IEEE Transactions on industrial electronics*, vol. 63, no. 2, pp. 1083–1095, 2015.

[28] W.-H. Chen, "Disturbance observer based control for nonlinear systems," *IEEE/ASME transactions on mechatronics*, vol. 9, no. 4, pp. 706–710, 2004.